CLIMATOLOGY

Weakening Atlantic Niño–Pacific connection under greenhouse warming

Fan Jia[1], Wenju Cai[2,3]*, Lixin Wu[2]*, Bolan Gan[2], Guojian Wang[2,3], Fred Kucharski[4], Ping Chang[5], Noel Keenlyside[6,7]

Sea surface temperature variability in the equatorial eastern Atlantic, which is referred to as an Atlantic Niño (Niña) at its warm (cold) phase and peaks in boreal summer, dominates the interannual variability in the equatorial Atlantic. By strengthening of the Walker circulation, an Atlantic Niño favors a Pacific La Niña, which matures in boreal winter, providing a precursory memory for El Niño–Southern Oscillation (ENSO) predictability. How this Atlantic impact responds to greenhouse warming is unclear. Here, we show that greenhouse warming leads to a weakened influence from the Atlantic Niño/Niña on the Pacific ENSO. In response to anomalous equatorial Atlantic heating, ascending over the equatorial Atlantic is weaker due to an increased tropospheric stability in the mean climate, resulting in a weaker impact on the Pacific Ocean. Thus, as greenhouse warming continues, Pacific ENSO is projected to be less affected by the Atlantic Niño/Niña and more challenging to predict.

INTRODUCTION

An Atlantic Niño, characterized by warm sea surface temperature (SST) anomalies in the equatorial east Atlantic, typically peaks in boreal summer and is the dominant mode of interannual variability in the equatorial Atlantic (*1*–*2*). Dynamics of an Atlantic Niño are somewhat similar to those of a Pacific El Niño, involving Bjerknes positive feedback. That is, initial warm SST anomalies in the equatorial eastern Atlantic lead to weaker trade winds, driving an eastward propagating equatorial oceanic downwelling Kelvin wave and a deeper thermocline, which, in turn, causes further warming in a coupled oceanic-atmospheric process (*3*–*5*). An Atlantic Niño promotes the occurrence of a Pacific La Niña in the ensuring winter (*6*–*14*). Specifically, the associated anomalous heating enhances local convections (fig. S1), inducing an intensified Walker circulation with an ascending branch over the Atlantic and a descending branch over the central Pacific during boreal summer (*8*–*11*). The latter causes equatorial easterly anomalies, triggering Bjerknes positive feedback in the equatorial Pacific, and the development of a La Niña event (*12*–*14*). The opposite operates for an Atlantic Niña to induce an El Niño.

An El Niño induced by an Atlantic Niña tends to have an anomaly center in the eastern Pacific (*14*), a type of event that is strong in strength and impact. The 1982 and 1997 extreme El Niño, the strongest events of the 20th century, were both preceded by an Atlantic Niña (table S1). The strongest La Niña events over the 20th century, 1988 and 1998, which caused billions in damage and loss of tens of thousands of lives (*15*–*16*), although associated with heat discharge from the El Niño in the previous year, were both preceded by an Atlantic Niño (table S1). Thus, the equatorial Atlantic forcing of El Niño–Southern Oscillation (ENSO) has provided an additional source of memory for ENSO prediction (*14*, *17*–*19*). In particular, incorporation of information on equatorial Atlantic SST markedly improves the prediction across boreal spring of major El Niño events (*14*, *18*). Therefore, how such Atlantic Niño–Pacific connection may change under greenhouse warming is not only an important scientific issue but also of practical utilities.

The Atlantic Niño–Pacific connection became statistically significant only after the late 1960s or early 1970s (*20*, *21*). Although early studies (*20*, *21*) suggested that the post-1970 connection may be linked to the negative phase of Atlantic multidecadal variability (AMV), inclusion of recent data shows that the connection persists through to the positive AMV phase since 2000 (Fig. 1A), possibly associated with decadal variability of a transbasin SST difference (*22*). An issue arises as to whether greenhouse warming contributes to the recent persistent connection. Here, we show that greenhouse warming leads to a weakening impact of Atlantic Niño/Niña on the Pacific Ocean.

RESULTS

Observed Atlantic Niño–Pacific connection

To depict the observed Atlantic Niño and its impact on the Pacific Ocean, we applied empirical orthogonal function (EOF) analysis to quadratically detrended SST anomalies (see "EOF analysis" section in Materials and Methods) averaged over boreal summer (June, July, and August or JJA0, where "0" refers to current year), in which an Atlantic Niño peaks. This yields a dominant principal pattern, and a principal component (PC) time series scaled to have a standard deviation (SD) of 1. In place of an index commonly taken as an average over a fixed area (*8*, *10*, *11*), we take the PC time series as the Atlantic Niño/Niña index, hereafter referred to as Atl-EOF index. Together with its associated pattern, the Atl-EOF index describes the anomaly pattern and evolution of the Atlantic Niño/Niña.

Given that the impact on the tropical Pacific reaches a maximum two seasons later (i.e., December, January, and February or D0JF1, where "1" refers to the following year), we measure the evolution of

[1]CAS Key Laboratory of Ocean Circulation and Waves, Institute of Oceanology, Center for Ocean Mega-Science, Chinese Academy of Sciences and Qingdao National Laboratory for Marine Science and Technology, 7 Nanhai Road, Qingdao 266071, China. [2]Key Laboratory of Physical Oceanography, Institute for Advanced Ocean Studies, Ocean University of China and Qingdao National Laboratory for Marine Science and Technology, 5 Yushan Road, Qingdao 266003, China. [3]Centre for Southern Hemisphere Oceans Research (CSHOR), CSIRO Oceans and Atmosphere, Hobart 7004, TAS, Australia. [4]Earth System Physics Section, Abdus Salam International Centre for Theoretical Physics, Trieste I-34100, Italy. [5]Department of Oceanography, Texas A&M University, 3146 TAMU, College Station, TX 77843, USA. [6]Geophysical Institute, University of Bergen and Bjerknes Centre for Climate Research, Allégaten 70, 5007 Bergen, Norway. [7]Nansen Environmental and Remote Sensing Center and Bjerknes Centre for Climate Research, Bergen, Norway.
*Corresponding author. Email: wenju.cai@csiro.au (W.C.); lxwu@ouc.edu.cn (L.W.)

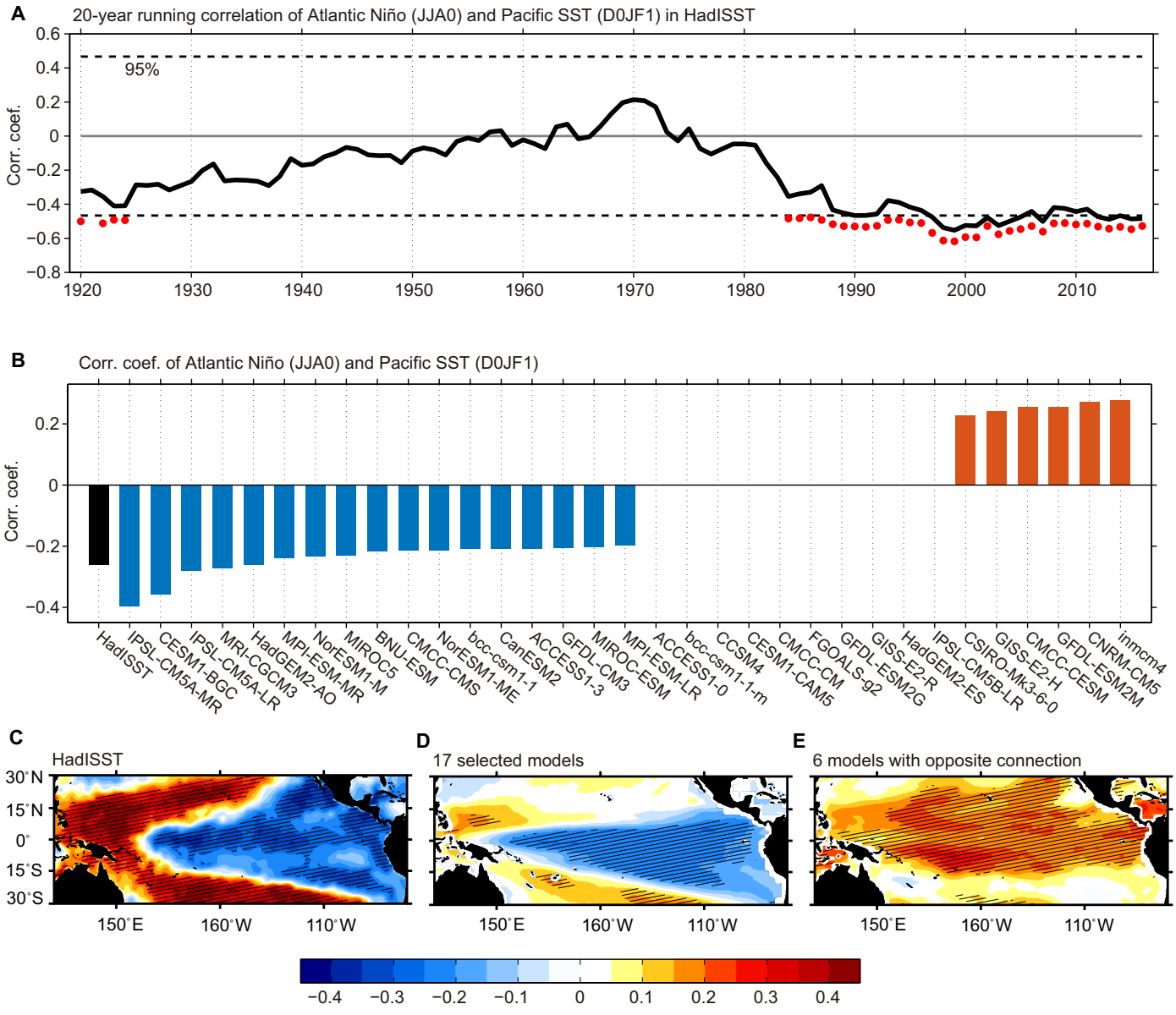

Fig. 1. Atlantic Niño–Pacific connection in observation and CMIP5 models. Correlation coefficients of the Atl-EOF index (JJA0) and the grid-point D0JF1 equatorial Pacific (5°S to 5°N and 160°E to 90°W) SST anomalies over a 20-year running window from 1900 to 2017 (recorded at end year of the window) in Hadley Centre Sea Ice and Sea Surface Temperature dataset (HadISST) (**A**) and over the 1900–1999 period in HadISST (black bar) and 33 CMIP5 models (**B**). Black solid line in (A) indicates area-averaged values of all the correlation coefficients in the equatorial Pacific. Red dots in (A) and bars in (B) indicate the average of only significant (more than 95% confidence level) correlation coefficients in the respective period (see "Sign-dependent average" section in Materials and Methods). Values of models that fail to produce any significant impact of Atlantic Niño on the equatorial Pacific are set to be zero in (B). Black dashed lines in (A) denote the value (±0.466) of the 95% confidence level based on Student's *t* test. (**C** to **E**) Spatial pattern of the correlation between the Atl-EOF index (JJA0) and the grid-point D0JF1 tropical Pacific SST anomalies over the 1900–1999 period based on HadISST (C), multimodel average of the 17 selected models (D), and multimodel average of the six models [orange bars in (B)] with opposite Atlantic Niño–Pacific connection (E). The values more than the 95% confidence level in (C) and the most robust features of ensemble where the mean exceeds 1 SD in (D) and (E) are hatched.

Atlantic Niño–Pacific connection by a correlation between the Atl-EOF index (i.e., PC1 at JJA0) and D0JF1 SST anomalies averaged over the equatorial Pacific (5°S to 5°N and 160°E to 90°W), in sliding 20-year windows with the result recorded in the last year of the window (black curve in Fig. 1A). Substantial fluctuations in the connection are seen, culminating in a persistent strong connection since the late 1960s. Considering that the relationship might not be statistically significant over the entire area of the equatorial Pacific, for each 20-year period, we calculated correlations with grid-point D0JF1 SST anomalies, but only significant grid-point correlations are averaged (red points in Fig. 1A) (see "Sign-dependent average" section in Materials and Methods). This confirms a persistent connection since the late 1960s.

The persistent connection reflects an important relationship between ENSO events (defined by National Ocean Atmosphere Administration) and the Atlantic Niño events (defined by a 0.5 SD

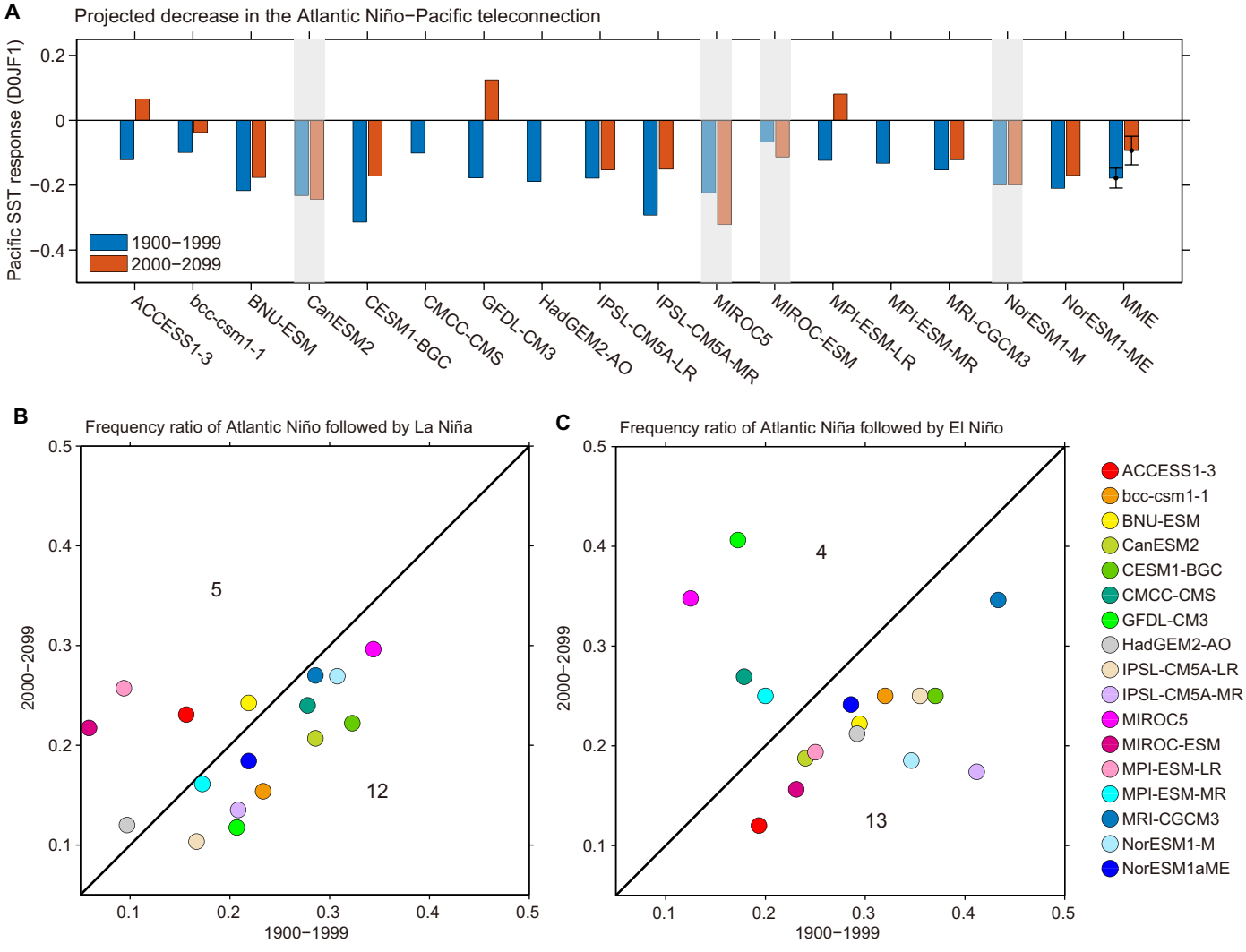

Fig. 2. Projected decrease in the Atlantic Niño–Pacific connection. (**A**) Comparison of the Pacific SST response (°C per SD) over the present-day (1900–1999; blue bars) and future (2000–2099; orange bars) 100-year periods in the 17 selected models. The four models that simulate an increase in response are grayed out. Error bars in the multimodel mean are calculated as 2 SDs (a 95% confidence interval based on normal distribution) of the 10,000 inter-realizations of a bootstrap method (see "Bootstrap test" section in Materials and Methods). The Pacific SST response is measured by regression coefficients of grid-point D0JF1 equatorial Pacific (5°S to 5°N and 160°E to 90°W) SST anomalies onto the Atl-EOF index (see "Sign-dependent average" section in Materials and Methods). (**B** and **C**) Comparison of the occurrence ratio of Atlantic Niño (Atl-EOF index > 0.5 SD) followed by La Niña (Niño3.4 index < −1 SD) over the total Atlantic Niño events (B) and that of Atlantic Niña (Atl-EOF index < −0.5 SD) followed by El Niño (Niño3.4 index >1 SD) over the total Atlantic Niña events (C) over the present-day (1900–1999; *x* axis) and future (2000–2099; *y* axis) 100-year periods in the 17 selected models. Numbers in the top left (bottom right) indicate the number of models that produce stronger (weaker) impact of Atlantic Niño/Niña on ENSO under future climate.

threshold of Atl-EOF index) (table S1). A total of 10 of 17 Atlantic Niño events are followed by La Niña events, including the more extreme events of 1988 and 1998. Eight of 17 Atlantic Niña events were followed by El Niño events, including the 1982, 1997, and 2015 extreme El Niño events. Because of the recent persistent correlation, a statistically significant Atlantic Niño–Pacific connection over the 1900–1999 period is seen in much of the equatorial Pacific (black bar in Fig. 1B and hashed area in Fig. 1C). Recent studies have shown that including this equatorial Atlantic influence improves ENSO prediction (*18*, *19*). Below, we examine the Atlantic Niño–Pacific connection under historical forcing and the representative concentration pathway 8.5 (RCP8.5) emission scenario in climate models participating in phase 5 of Coupled Model Intercomparison Project (CMIP5) (see "Observed and CMIP5 data" section in Materials and Methods).

Simulation of the Atlantic Niño–Pacific connection

We identify CMIP5 models that are able to simulate the Atlantic Niño–Pacific connection. As for the observations, we applied EOF analysis to JJA0 SST anomalies quadratically detrended over the full 200 years (1900–2099). This allows our models to have an Atlantic Niño pattern that is different from the observed and different from one model to another. As in our analysis of the observed data, we correlate the Atl-EOF index (JJA0 PC time series) with grid-point D0JF1 equatorial Pacific SST anomalies over the 1900–1999 period, referred to as the present-day climate (see "Model selection" section in Materials and Methods). We use an average correlation over grid points with a significant coefficient to evaluate whether a model is able to simulate the Atlantic Niño–Pacific connection (see "Sign-dependent average" section in Materials and Methods). These approaches are

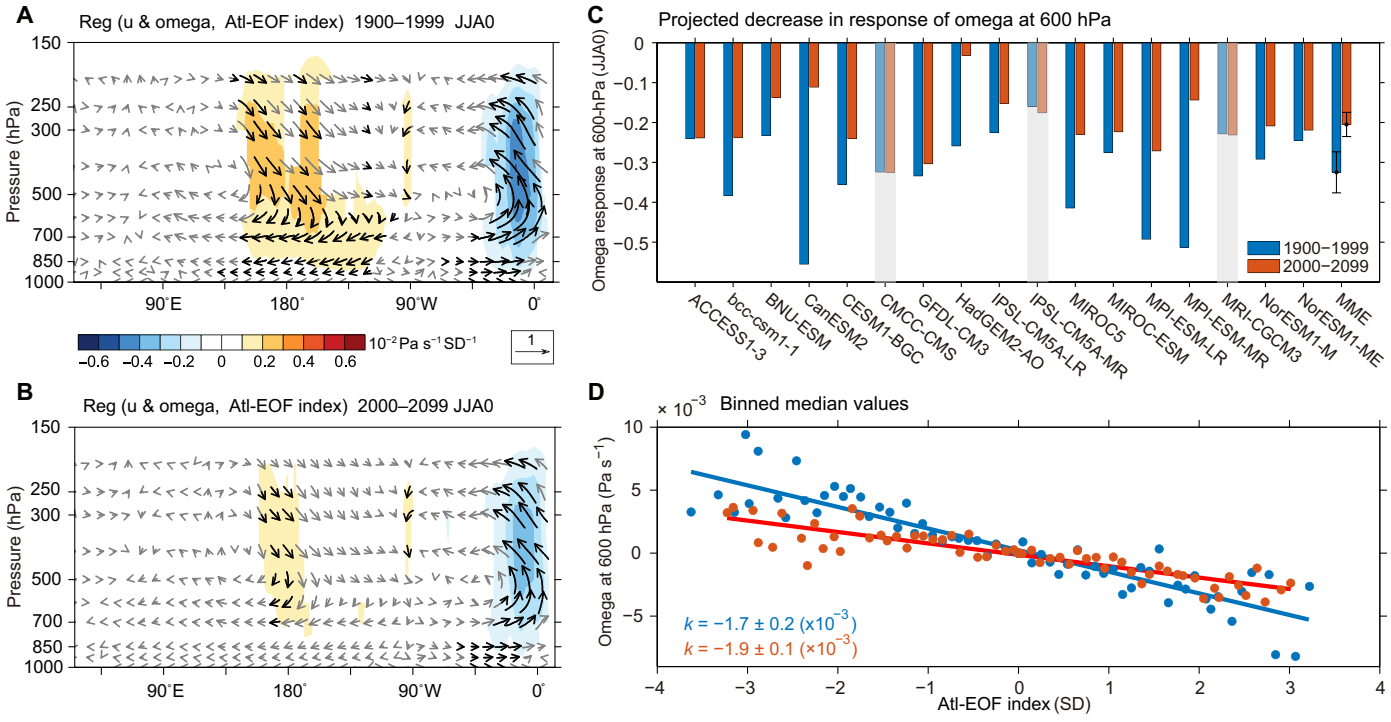

Fig. 3. Projection of decreased response to a diabatic equatorial Atlantic heating. Multimodel (the 17 selected models) average of boreal summer (JJA0) regression of equatorial (10°S to 10°N) vertical atmospheric velocity (pascals per second; color) and equatorial atmospheric flow vectors (zonal wind and vertical velocity scaled by a factor of 300) onto the Atl-EOF index of the present-day (1900–1999) (**A**) and future (2000–2099) (**B**) 100-year periods. Values exceeding 1 SD are shown in shaded contour and black vectors. The color map and reference vector are labeled in the middle of (A) and (B). (**C**) Comparison of vertical velocity response to the Atl-EOF index over the present-day (blue bars) and future (orange bars) 100-year periods in the 17 selected models. The three models that simulate an increase in response are marked in gray. Error bars in the multimodel mean are calculated as 2 SDs (the 95% confidence interval based on normal distribution) of the 10,000 inter-realizations of a bootstrap method (see "Bootstrap test" section in Materials and Methods). The vertical velocity response is measured by the regression coefficients (pascals per second per SD) of the JJA0 vertical velocity anomalies at 600 hPa averaged over the equatorial Atlantic (5°S to 5°N and 45°W to 20°E) and the respective Atl-EOF index. (**D**) Responses of JJA0 vertical velocity anomalies at 600 hPa averaged over the equatorial Atlantic (5°S to 5°N and 45°W to 20°E) (pascals per second) to JJA0 Atl-EOF index using all samples of 17 selected models. The vertical velocity anomalies are binned in 0.1 SD. Atl-EOF index intervals and the median vertical velocity anomaly and index are identified for each bin (dots). Blue and red dots indicate values in the present-day and future 100-year periods, respectively. The corresponding linear fitting lines (with the values of the slopes plus and minus the 95% confidence values from the Student's *t* test) are also shown.

adapted to select as many models as possible. A total of 17 models simulate a connection reminiscent of the observed, although the locations of correlation could be different (Fig. 1, B and D). Ten models produce no such connection, whereas six models produce an opposite connection (Fig. 1, B and E), consistent with previous findings that the Atlantic Niño–Pacific connection is not simulated by all models (*23*–*25*).

The Atlantic Niño pattern simulated by the 17 selected models is comparable to that in the observation, although they are generally weaker and more equatorially confined than the observed pattern (fig. S2). Our approach is to examine how the Atlantic Niño–Pacific connection, as simulated by a model, may change under greenhouse warming. An intermodel relationship shows that correlation over the full 100-year period increases with the maximum of 20-year sliding correlations over the same 100 years (fig. S3). Thus, as in the observed data, the correlation coefficient over the 100-year period is contributed by period(s) of large statistically significant correlation embedded in multidecadal fluctuations. The 17 models in aggregation produce the observed forcing of Atlantic Niño on the Pacific, i.e., an Atlantic Niño leads to a Pacific La Niña and an Atlantic Niña leads to a Pacific El Niño (compare figs. S1 and S4), through the Pacific Bjerknes feedback involving winds, SST, and the thermocline.

Weakened Atlantic Niño–Pacific connection in future climate

We compare the Atlantic Niño–Pacific connection in the 17 selected models between the present period and the future period (2000–2099). There is no consistent change in variability of Atlantic Niño (fig. S5). For each period, we regress grid-point SST anomalies onto the Atl-EOF index, yielding the response of the equatorial Pacific grid-point SST (D0JF1), per SD of the Atl-EOF time series. We obtain an average of regression coefficients over the grid points with statistically significant correlation coefficients above the 95% confidence level (see "Sign-dependent average" section in Materials and Methods). A total of 13 of 17 selected models, or 76%, generate a reduced response (Fig. 2A). Aggregated over the 17 models, there is a reduction of 47.8%, from –0.178°C SD^{-1} in the present-day climate to –0.093°C SD^{-1} in the future climate. This reduction is statistically significant above the 99% confidence level, according to the bootstrap method (see "Bootstrap test" section in Materials and Methods) (fig. S6A), supported by a comparison in the evolution of the Atlantic Niño–Pacific connection for the two periods (fig. S4), showing a conspicuous weakening in the connection.

The reduced connection translates to a general reduction in Atlantic Niño/Niña events that are followed by Pacific Niña/Niño events. Using 0.5 SD as a threshold to define Atlantic Niño

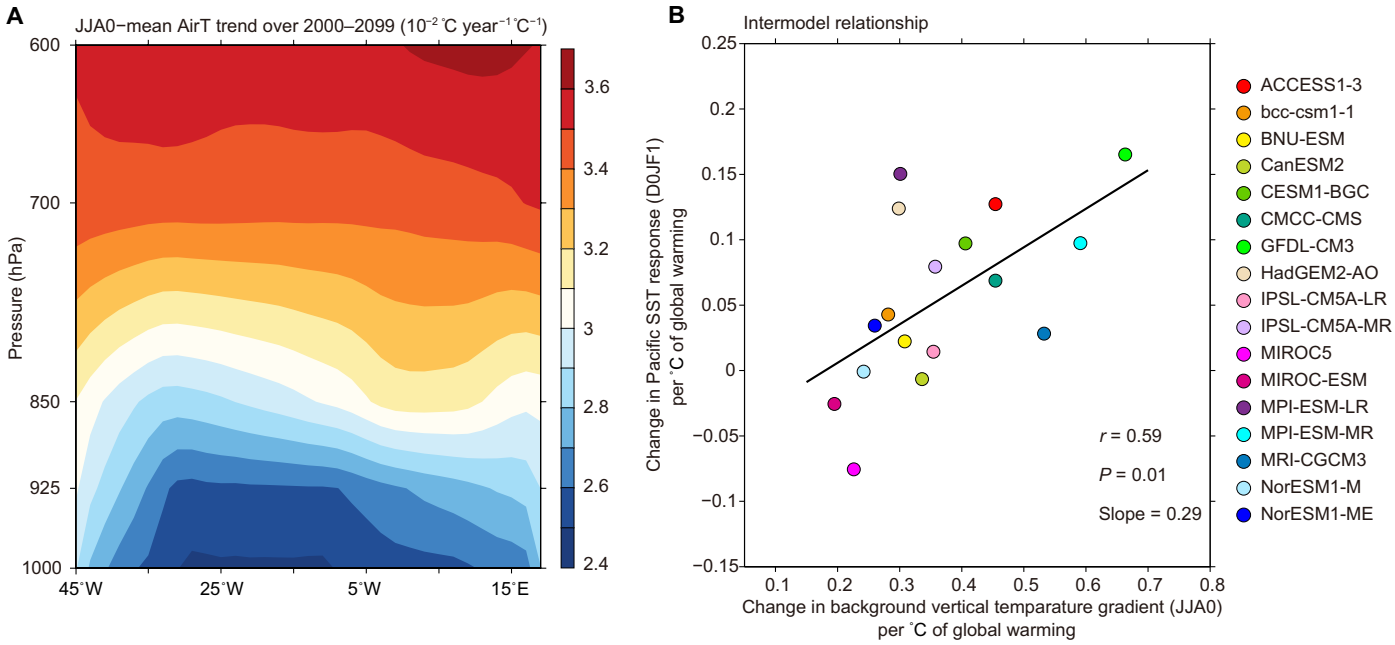

Fig. 4. Mechanism for the projected decrease in the Atlantic Niño–Pacific connection. (**A**) Warming trend of the boreal summer mean (JJA0) air temperature (AirT) over the equatorial Atlantic (5°S to 5°N and 45°W to 20°E) at different levels during 2000–2099. (**B**) Intermodel relationship between the change (between future and present-day climates) of boreal summer mean (JJA0) atmospheric stratification and the Pacific SST response. The atmospheric stratification is calculated as the difference between the boreal summer mean (JJA0) temperature at 600 hPa and the temperature at 925 hPa, both averaged over the equatorial Atlantic. The linear fit (solid line) is displayed together with the correlation coefficient *r*, slope, and *P* value from the regression. To enhance the intermodel comparability, we scale both the warming trend in (A) and the changes in (B) by the increase in global mean temperature over the present-day and future periods.

(|Atl-EOF index| > 0.5 SD) events and 1.0 SD to define ENSO (|Niño3.4| > 1.0 SD), most models generate a decreased occurrence ratio of Atlantic Niño (Niña) followed by La Niña (El Niño) in future climate (Fig. 2, B and C). This reduction generally translates into a decreased occurrence ratio in future climate in terms of Atlantic Niño followed by strong La Niña or Atlantic Niña followed by strong El Niño (fig. S6, B and C), in which a strong El Niño and strong La Niña is defined as when the amplitude of SST anomalies in their respective centers are greater than 1.5 and 1.75 SDs, respectively (see "E-index and C-index" section in Materials and Methods, describing SST variability at eastern Pacific for strong El Niño and at central Pacific for strong La Niña). Thus, the projected increase in frequency of strong El Niño and La Niña events under greenhouse warming, reported by other studies (*26*–*28*), occurs despite a decreased influence from the Atlantic, reinforcing the role of the future mean state changes of the Pacific Ocean in the projected ENSO changes (*26*–*28*).

A weakened connection driven by a more stable troposphere

The Atlantic Niño–Pacific connection is underpinned by the response of equatorial Atlantic convection to the Atlantic Niño/Niña (*8*, *10*, *11*), manifested in a rising motion commencing approximately 600 hPa in both the present day and future climates (Fig. 3, A and B). In response to diabatic heating anomalies, the response of vertical velocity is smaller in the future than in the present-day climate in the majority of models (Fig. 3C), with 14 of 17 models generating a weaker response in the future climate. Aggregated over all models, there is a statistically significant weakening in the multimodel response of the vertical velocity to the Atl-EOF index, by as much as 47%, as can be seen from comparison of slopes for the present-day and future climates (Fig. 3D). The weakened convection response is accompanied by a decreased precipitation response to Atlantic Niño/Niña under future climate, with a strong (14 of 17) intermodel consensus (fig. S7).

Under global warming, the midtroposphere warms faster than the near-surface levels (Fig. 4A) (*29*, *30*), reducing the boreal summer mean negative vertical temperature gradient, defined as the difference between the boreal summer mean temperature at 600 hPa and the temperature at 925 hPa. This weakened negative vertical gradient is seen in all selected models (Fig. 4B). It is this more stable troposphere that weakens the convective response, leading to the weakened Atlantic Niño–Pacific connection; models that generate a larger reduction in the background temperature gradient tend to simulate a weaker boreal winter Pacific SST response (Fig. 4B), and the tendency is statistically significant. The weakened connection occurs despite a strengthening ocean-atmosphere coupling in the equatorial Pacific under greenhouse warming (*28*), which would otherwise enhance the connection.

The increased tropospheric stability under greenhouse warming also occurs in the equatorial Pacific. In the Pacific, however, this is offset by an increased probability of atmospheric deep convection over the equatorial eastern Pacific, where the fastest warming in the tropics occurs (fig. S8), leading to an increased rainfall response of SST anomalies under greenhouse warming (*26*). In the equatorial Atlantic, SST warms slower and more uniform than that in the equatorial Pacific (fig. S8), and the damping effect of increased atmosphere stability dominates.

Implications for ENSO prediction

We further confirm the above result by two sets of 20-member experiments using a coupled model of intermediate complexity

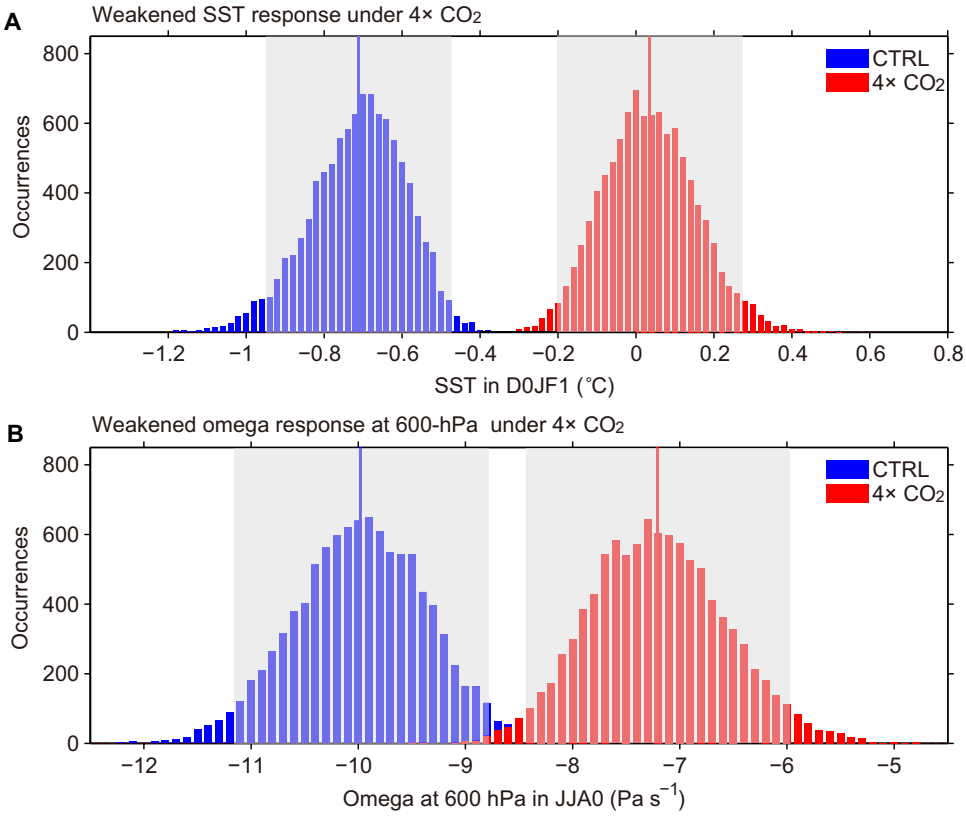

Fig. 5. Weakened Atlantic Niño–Pacific teleconnection in the CAM3.1-RGO experiments. Histograms of 10,000 realizations of the bootstrap method for the Pacific SST response (**A**) and vertical velocity anomalies at 600 hPa (**B**) in the initial experiments under control (blue) and 4× CO_2 (red) (see "Model experiments" section in Materials and Methods). The Pacific SST response is measured by the area-averaged D0JF1 equatorial Pacific (5°S to 5°N and 160°E to 90°W) SST anomalies, and the vertical velocity anomalies at 600 hPa are averaged over the equatorial Atlantic (5°S to 5°N and 45°W to 20°E) during boreal summer (pascals per second; JJA0). The blue and red vertical lines indicate the mean values of 10,000 inter-realizations for the present-day and future periods, respectively. The gray shaded regions indicate the respective doubled SDs (the 95% confidence interval based on normal distribution) of the 10,000 inter-realization (see "Bootstrap test" section in Materials and Methods).

(see "Model description" section in Materials and Methods), under a control [355 parts per million (ppm), constant] and 4× CO_2 (1420 ppm) concentration (see "Model experiments" section in Materials and Methods). The 4× CO_2 leads to a weakening in the mean vertical temperature gradient of 0.72 K per °C of global warming. In each fully coupled model setting, the observed Atlantic Niño pattern (fig. S1A) is amplified by a factor of 4 to increase a response signal, imposed as an initial condition on the first day of June with an added stochastic noise. We analyze the response to the initial condition in the ensuing year. Aggregated over the 20 experiments, under the control condition, the Atlantic Niño–Pacific connection is produced, but under the 4× CO_2 condition, the connection weakens markedly, commencing from a much reduced vertical velocity at 600 hPa (Fig. 5). The result, together with the experiment design in which the Atlantic forcing of the Pacific Ocean is realized by an initial condition, underscores a reduction in the Atlantic memory for ENSO prediction.

DISCUSSION

In summary, the Atlantic Niño–Pacific Ocean connection is likely to weaken under greenhouse warming, as the midtroposphere warms faster than the near surface, increasing the thermal stability of the atmosphere. This leads to a reduced response of equatorial Atlantic convection to SST anomalies, hence a weakened connection to the Pacific Ocean. Although bias exists in the CMIP5 models, there is no evidence to suggest that either the warm SST bias in the equatorial Atlantic mean state (fig. S9A; intermodel correlation between biases and simulated changes, −0.13) or the bias of Atlantic Niño–Pacific connection itself (fig. S9B; intermodel correlation between biases and simulated changes, 0.01) contributes to the weakened Pacific SST response under future climate. Our result suggests that the recent strengthening in the Atlantic Niño–Pacific Ocean connection may not be induced by greenhouse warming. Furthermore, the projected future increase in the frequency of extreme El Niño and La Niña events (*26*–*28*) occurs despite the projected weakening influence from the equatorial Atlantic, but the prediction of these future extreme ENSO events is likely to be more challenging as the memory from the Atlantic forcing weakens.

MATERIALS AND METHODS

Observed and CMIP5 data

The observed monthly SST, three-dimensional oceanic temperature and atmospheric fields (three-dimensional velocities and precipitation) were from the Hadley Centre Sea Ice and Sea Surface Temperature dataset (HadISST; 1900–2017) (*31*), the Ocean Reanalysis System version 4 (ORAS4; 1976–2015) (*32*), and the National Center for Environmental Prediction (NCEP)/National Center for Atmospheric

Research (NCAR) reanalysis 1 (1976–2015) (*33*), respectively. We analyzed 33 CMIP5 models' historical simulations over the 1900–1999 period (present-day climate) and RCP8.5 experiments over the 2000–2099 period (future climate) (table S2) (*34*). The former runs were forced by the observed atmospheric composition in the 20th century, and the latter experiments were forced by an escalating radiative force throughout the 21st century (reaching approximately 8.5 W m^{-2} in 2100).

EOF analysis

To depict the Atlantic Niño unique to each model, we applied an EOF analysis to quadratically detrended JJA0 SST anomalies of tropical Atlantic (20°S to 20°N and 60°W to 20°E) to capture the observed and modeled Atlantic Niño (*3*, *21*, *23*). We did not use the commonly used ATL3 index defined as the SST anomaly in the central-eastern equatorial Atlantic (3°S to 3°N and 20°W to 0°E). Although this index captures the observed Atlantic Niño, it might be inappropriate for CMIP5 outputs because the pattern of Atlantic Niño varies substantially among models. For CMIP5 models, the EOF analysis was applied to the full 200-year period (1900–2099) to represent the overall simulations of Atlantic Niño in both the present-day and future climates. Anomalies here were computed by removing seasonal cycles referenced to the long-term mean and quadratic trends from the monthly data (for all the CMIP5 outputs, the anomalies were obtained on the basis of the full 200-year period). Following (*13*), the impact of ENSO was excluded first through linear regressions onto Niño3.4 SST (5°S to 5°N and 170°W to 120°W) in the previous D-1JF0.

Sign-dependent average

The correlation or regression coefficients in the equatorial Pacific region (5°S to 5°N and 160°E to 90°W) were averaged as follows. First, only correlation (or regression) coefficients at grid points that are statistically significant (more than 95% confidence level) were considered. Coefficients that are not significant were discarded. We then examined whether the retained values in terms of a whole-region average. If negative, then only the significant negative coefficients were averaged, or if positive, then only the significant positive coefficients were averaged. If there were no significant coefficients at any grid points in the equatorial Pacific region (5°S to 5°N and 160°E to 90°W), the result was set to be zero (see Fig. 1A).

Model selection

The normalized PC time series (defined as Atl-EOF index) was used to represent the temporal variability of Atlantic Niño. Although the Atlantic Niño was the dominant mode (EOF1) of tropical Atlantic in observations, it may appear as the second mode in some CMIP5 models (*23*). We thus calculated linear correlation of the leading two PCs and the following D0JF1 equatorial Pacific (5°S to 5°N and 160°E to 90°W) SST anomaly at each grid point, and computed the sign-dependent average correlations. Since the observed Atlantic Niño (JJA0) and Pacific SST (D0JF1) were negatively correlated, the minimum value between the correlation results of the two PCs was taken as a measurement of the Atlantic Niño–Pacific connection, with the corresponding 200-year PC time series being the model Atl-EOF index (table S2).

Bootstrap test

We used a bootstrap method (*35*) to examine whether the decreased response of Pacific SST is statistically significant. The 17 sign-dependent average regressions (R_SST hereafter) in the present-day and future climate periods from the 17 selected models were resampled randomly to construct respective 10,000 realizations of mean R_SST values. In this random resampling process, any model can be selected again. The doubled SDs of the 10,000 inter-realizations of mean R_SST for the present-day and future climate periods were 0.03 and 0.056, respectively. The decreased R_SST in the future period (0.091) is greater than the sum of these two doubled SD values (0.086), indicating statistical significance above the 99% confidence level (Fig. 2A). The same bootstrap tests were also applied to check the response of vertical velocity to diabatic heating (Fig. 3C) and the model experiments results (Fig. 5).

E-index and C-index

We applied the EOF analysis to the quadratically detrended D0JF1 SST anomalies of equatorial Pacific (15°S to 15°N and 140°E to 80°W) in the 17 selected models, covering the 200-year period (1900–2099). The PC time series was scaled to have an SD of 1. We also made sure that the PC1 and PC2 correspond to the respective positive phase of EOF1 (warm anomaly center in the central eastern Pacific) and EOF2 (a warm anomaly center in the central Pacific and a cool anomaly aside). The temporal variability of the central Pacific–ENSO and eastern Pacific–ENSO (*36*) can be described by a C-index [(PC1 + PC2)/2] and an E-index [(PC1 − PC2)/2], respectively (*37*).

Model description

We further examined our mechanism using an intermediate climate model (*38*, *39*), which is a fully coupled system consisting of the Community Atmosphere Model version 3.1 (CAM3.1) and a 1.5-layer reduced-gravity ocean (RGO) model with flux corrections (CAM3.1-RGO model hereafter). The atmospheric component is part of the Community Climate System Model version 3 developed at the NCAR. It was based on a Eulerian spectral dynamical core, with a T42 horizontal resolution and 26 vertical levels. The land surface processes in CAM3.1 were represented by the Community Land Model version 3, a fully interactive land model. The oceanic component was an extended Zebiak-Cane type of 1.5-layer RGO model (*40*, *41*). The active upper ocean layer was divided into a fixed-depth mixed layer to simulate SST variation and a subsurface layer to parameterize the entrained subsurface temperature through the multivariate linear relationship with thermocline depth. The ocean model covers a global domain (80°S to 80°N and 0°E to 360°E) with 1° latitude by 2° longitude resolution, which contains variability off the equatorial band [see more details in (*36*)]. The CAM3.1-RGO model was proved to be a useful and efficient tool to study climate change related questions (*38*, *39*, *42*), as the effects of different ocean and atmosphere dynamic processes are easier to decipher in this model than the CGCMs.

Model experiments

We first conducted two simulations with long integration using CAM3.1-RGO, including a 500-year control run (control) and a 400-year quadrupled CO_2 concentration run (4× CO_2). The latter starts from the 100th year of control with a sudden quadrupling (1420 ppm) of CO_2 concentration. Then, from the respective equilibrium state of control and 4× CO_2, two sets of initial-value ensemble runs were carried out. For each member of the experiments, the quadrupled Atlantic Niño SST pattern derived from observations (fig. S1A) was initiated over the tropical Atlantic (20°S to 20°N) region on the first day of June and tracked for 1 year within the fully coupled environment.

A total of 20-member ensemble experiments were performed for each set, with each member starting from a slightly different initial condition. We also carried out two parallel sets of 20-member ensemble experiments, where zero SST anomalies were initiated. The differences between the corresponding sets of experiments are the responses to the imposed Atlantic Niño SST anomalies. The result confirms a decreased Atlantic Niño–Pacific connection. Further, the system's memory of the Atlantic's initial conditions is likely to be weaker in the future.

SUPPLEMENTARY MATERIALS

Supplementary material for this article is available at http://advances.sciencemag.org/cgi/content/full/5/8/eaax4111/DC1

Fig. S1. Observed development of the Atlantic Niño–Pacific connection.
Fig. S2. Comparison of Atlantic Niño patterns in observation and 17 selected models.
Fig. S3. Intermodel relationship of Atlantic Niño–Pacific teleconnection over 100 years and its multidecadal fluctuations.
Fig. S4. Modeled development of the Atlantic Niño–Pacific teleconnection.
Fig. S5. Impact of the Atlantic Niño amplitude change on the Pacific SST response.
Fig. S6. Projected decrease in the Atlantic Niño–Pacific connection in terms of bootstrap test and extreme ENSO.
Fig. S7. Projection of decreased precipitation response to a diabatic equatorial Atlantic heating.
Fig. S8. Projected warming pattern of equatorial Pacific and Atlantic Ocean.
Fig. S9. Impact of model biases on the Pacific SST response.
Table S1. Observed relationship between ENSO events and the Atlantic Niño.
Table S2. CMIP5 models and their EOF modes of tropical Atlantic used in this study.

REFERENCES AND NOTES

1. J. Merle, Variabilité thermique annuelle et interannuelle de l'océan Atlantique équatorial Est. L'hypothèse d'un "El Niño" Atlantique. *Oceanol. Acta* **3**, 209–220 (1980).
2. S. E. Zebiak, Air-Sea interaction in the equatorial Atlantic region. *J. Climate* **6**, 1567–1586 (1993).
3. P. Chang, T. Yamagata, P. Schopf, S.-K. Behera, J. Carton, W. S. Kessler, G. Meyers, T. Qu, F. Schott, S. Shetye, S.-P. Xie, Climate fluctuations of tropical coupled systems-the role of ocean dynamics. *J. Climate* **19**, 5122–5174 (2006).
4. N. S. Keenlyside, M. Latif, Understanding equatorial Atlantic interannual variability. *J. Climate* **20**, 131–142 (2007).
5. I. Polo, A. Lazar, B. Rodriguez-Fonseca, S. Arnault, Oceanic Kelvin waves and tropical Atlantic intraseasonal variability: 1. Kelvin wave characterization. *J. Geophys. Res.* **113**, C07009 (2008).
6. D. Dommenget, V. Semenov, M. Latif, Impacts of the tropical Indian and Atlantic Oceans on ENSO. *Geophys. Res. Lett.* **33**, L11701 (2006).
7. C. Wang, An overlooked feature of tropical climate: Inter-Pacific-Atlantic variability. *Geophys. Res. Lett.* **33**, L12702 (2006).
8. B. Rodríguez-Fonseca, I. Polo, J. García-Serrano, T. Losada, E. Mohino, C. R. Mechoso, F. Kucharski, Are Atlantic Niños enhancing Pacific ENSO events in recent decades? *Geophys. Res. Lett.* **36**, L20705 (2009).
9. T. Losada, B. Rodríguez-Fonseca, I. Polo, S. Janicot, S. Gervois, F. Chauvin, P. Ruti, Tropical response to the Atlantic equatorial mode: AGCM multimodel approach. *Climate Dynam.* **35**, 45–52 (2010).
10. H. Ding, N. S. Keenlyside, M. Latif, Impact of the equatorial Atlantic on the El Niño Southern Oscillation. *Climate Dynam.* **38**, 1965–1972 (2012).
11. I. Polo, M. Martín-Rey, B. Rodríguez-Fonseca, F. Kucharski, C. R. Mechoso, Processes in the Pacific La Niña onset triggered by the Atlantic Niño. *Climate Dynam.* **44**, 115–131 (2015).
12. M. F. Jansen, D. Dommenget, N. S. Keenlyside, Tropical atmosphere-ocean interactions in a conceptual framework. *J. Climate* **22**, 550–567 (2009).
13. M. Martín-Rey, I. Polo, B. Rodríguez-Fonseca, F. Kucharski, Changes in the interannual variability of the tropical Pacific as a response to an equatorial Atlantic forcing. *Sci. Mar.* **76**, 105–116 (2012).
14. Y.-G. Ham, J.-S. Kug, J.-Y. Park, Two distinct roles of Atlantic SSTs in ENSO variability: North tropical Atlantic SST and Atlantic Niño. *Geophys. Res. Lett.* **40**, 4012–4017 (2013).
15. M. C. Bove, J. B. Eisner, C. W. Landsea, X. Niu, J. J. O'Brien, Effect of El Niño on U.S. landfalling hurricanes, revisited. *Bull. Am. Meteorol. Soc.* **79**, 2477–2482 (1998).
16. G. D. Bell, M. S. Halpert, V. E. Kousky, M. E. Gelman, C. F. Ropelewski, A. V. Douglas, R. C. Schnell, Climate assessment for 1998. *Bull. Am. Meteorol. Soc.* **80**, –1040 (1999).
17. B. Dong, R. T. Sutton, Enhancement of ENSO variability by a weakened Atlantic thermohaline circulation in a coupled GCM. *J. Climate* **20**, 4920–4939 (2007).
18. N. S. Keenlyside, H. Ding, M. Latif, Potential of equatorial Atlantic variability to enhance El Niño prediction. *Geophys. Res. Lett.* **40**, 2278–2283 (2013).
19. M. Martín-Rey, B. Rodríguez-Fonseca, I. Polo, Atlantic opportunities for ENSO prediction. *Geophys. Res. Lett.* **42**, 6802–6810 (2015).
20. M. Martín-Rey, B. Rodríguez-Fonseca, I. Polo, F. Kucharski, On the Atlantic-Pacific Niños connection: A multidecadal modulated mode. *Climate Dynam.* **43**, 3163–3178 (2014).
21. M. Martín-Rey, I. Polo, B. Rodríguez-Fonseca, T. Losada, A. Lazar, Is there evidence of changes in tropical Atlantic variability modes under AMO phases in the observational record? *J. Climate* **31**, 515–536 (2018).
22. X. Li, S.-P. Xie, S. T. Gille, C. Yoo, Atlantic induced pan-tropical climate change over the past three decades. *Nat. Clim. Change* **6**, 275–279 (2016).
23. I. Richter, S.-P. Xie, S. K. Behera, T. Doi, Y. Masumoto, Equatorial Atlantic variability and its relation to mean state biases in CMIP5. *Climate Dynam.* **42**, 171–188 (2014).
24. F. Kucharski, F. S. Syed, A. Burhan, I. Farah, A. Gohar, Tropical Atlantic influence on Pacific variability and mean state in the twentieth century in observations and CMIP5. *Climate Dynam.* **44**, 881–896 (2015).
25. I. Ott, K. Romberg, J. Jakobeit, Teleconnections of the tropical Atlantic and Pacific Oceans in a CMIP5 model ensemble. *Climate Dynam.* **44**, 3043–3055 (2015).
26. W. Cai, S. Borlace, M. Lengaigne, P. van Rensch, M. Collins, G. Vecchi, A. Timmermann, A. Santoso, M. J. McPhaden, L. Wu, M. H. England, G. Wang, E. Guilyardi, F.-F. Jin, Increasing frequency of extreme El Niño events due to greenhouse warming. *Nat. Clim. Change* **4**, 111–116 (2014).
27. W. Cai, G. Wang, A. Santoso, M. J. McPhaden, L. Wu, F.-F. Jin, A. Timmermann, M. Collins, G. Vecchi, M. Lengaigne, M. H. England, D. Dommenget, K. Takahashi, E. Guilyardi, Increased frequency of extreme La Niña events under greenhouse warming. *Nat. Clim. Change* **5**, 132–137 (2015).
28. W. Cai, G. Wang, B. Dewitte, L. Wu, A. Santoso, K. Takahashi, Y. Yang, A. Carréric, M. J. McPhaden, Increased variability of eastern Pacific El Niño under greenhouse warming. *Nature* **564**, 201–206 (2018).
29. R. J. Allen, S. C. Sherwood, Warming maximum in the tropical upper troposphere deduced from thermal winds. *Nat. Geosci.* **1**, 399–403 (2008).
30. N. C. Johnson, S.-P. Xie, Changes in the sea surface temperature threshold for tropical convection. *Nat. Geosci.* **3**, 842–845 (2010).
31. N. A. Rayner, D. E. Parker, E. B. Horton, C. K. Folland, L. V. Alexander, D. P. Rowell, E. C. Kent, A. Kaplan, Global analyses of sea surface temperature, sea ice, and night marine air temperature since the late nineteenth century. *J. Geophys. Res.* **108**, 4407 (2003).
32. M. A. Balmaseda, K. Mogensen, A. T. Weaver, Evaluation of the ECMWF ocean reanalysis system ORAS4. *Q. J. Roy. Meteorol. Soc.* **139**, 1132–1161 (2013).
33. E. Kalnay, M. Kanamitsu, R. Kistler, W. Collins, D. Deaven, L. Gandin, M. Iredell, S. Saha, G. White, J. Woollen, Y. Zhu, A. Leetmaa, R. Reynolds, M. Chelliah, W. Ebisuzaki, W. Higgins, J. Janowiak, K. C. Mo, C. Ropelewski, J. Wang, R. Jenne, D. Joseph, The NCEP/NCAR 40-year reanalysis project. *Bull. Am. Meteorol. Soc.* **77**, 437–471 (1996).
34. K. E. Taylor, R. J. Stouffer, G. A. Meehl, An overview of CMIP5 and the experiment design. *Bull. Am. Meteorol. Soc.* **93**, 485–498 (2012).
35. P. C. Austin, J. V. Tu, Bootstrap methods for developing predictive models. *Am. Stat.* **58**, 131–137 (2004).
36. K. Ashok, S. K. Behera, S. A. Rao, H. Weng, T. Yamagata, El Niño Modoki and its possible teleconnection. *J. Geophys. Res.* **112**, C11007 (2007).
37. K. Takahashi, B. Dewitte, Strong and moderate nonlinear El Niño regimes. *Climate Dynam.* **46**, 1627–1645 (2016).
38. Y. Fang, "A coupled model study of the remote influence of ENSO on tropical Atlantic SST variability," Ph.D. thesis, Texas A&M University, 93 pp. (2005).
39. J. C. H. Chiang, Y. Fang, P. Chang, Interhemispheric thermal gradient and tropical Pacific climate. *Geophys. Res. Lett.* **35**, L14704 (2008).
40. S. E. Zebiak, M. A. Cane, A model El Niño–Southern Oscillation. *Mon. Wea. Rev.* **115**, 2262–2278 (1987).
41. A. C. Clement, R. Seager, M. A. Cane, S. E. Zebiak, An ocean dynamical thermostat. *J. Climate* **9**, 2190–2196 (1996).
42. F. Jia, L. Wu, B. Gan, W. Cai, Global warming attenuates the tropical Atlantic-Pacific teleconnection. *Sci. Rep.* **6**, 20078 (2016).

Acknowledgments

Funding: F.J. is supported by the National Natural Science Foundation of China (NSFC) projects (41876008, 41490641, and 41490640). W.C. is supported by National Key R&D Program of China (2018YFA0605700). L.W. and B.G. are supported by NSFC projects (41490643, 41490640, 91858102, and U1606402). W.C. and G.W. are also supported by CSHOR and the Earth System and Climate Change Hub of the Australian Government's National Environment Science Program. CSHOR is a joint research Centre for Southern Hemisphere Oceans Research between QNLM and CSIRO. **Author contributions:** F.J. conceived the study in discussion with W.C. and L.W. F.J. conducted experiments and analysis and wrote the initial manuscript with W.C. All authors contributed to interpreting results, discussion of the associated dynamics, and improvement of this paper. **Competing interests:** The authors declare that they have no

competing interests. **Data and materials availability:** All data needed to evaluate the conclusions in the paper are present in the paper, which can be downloaded from the following: HadISST v1.1, www.metoffice.gov.uk/hadobs/hadisst/; ORAS4, https://climatedataguide.ucar.edu/climate-data/oras4-ecmwf-ocean-reanalysis-and-derived-ocean-heat-content; NCEP/NCAR reanalysis, www.esrl.noaa.gov/psd/data/gridded/data.ncep.reanalysis.derived.html; and CMIP5 database, www.ipcc-data.org/sim/gcm:monthly/AR5/. Codes of the CAM3.1-RGO and additional data related to this paper may be requested from the authors.

Submitted 20 March 2019
Accepted 12 July 2019
Published 21 August 2019
10.1126/sciadv.aax4111

Citation: F. Jia, W. Cai, L. Wu, B. Gan, G. Wang, F. Kucharski, P. Chang, N. Keenlyside, Weakening Atlantic Niño–Pacific connection under greenhouse warming. *Sci. Adv.* **5**, eaax4111 (2019).

Weakening Atlantic Niño–Pacific connection under greenhouse warming

Fan Jia, Wenju Cai, Lixin Wu, Bolan Gan, Guojian Wang, Fred Kucharski, Ping Chang and Noel Keenlyside

Sci Adv **5** (8), eaax4111.
DOI: 10.1126/sciadv.aax4111